DAVENPORT, H. (1952). *The Higher Arithmetic*, pp. 130-140. London: Hutchinson.
HARDY, G. H. & WRIGHT, E. M. (1979). *An Introduction to the Theory of Numbers*, 5th ed. Oxford Univ. Press.
HARKER, D. (1978). *Proc. Natl Acad. Sci. USA*, **75**, 5264-5267.
HAUPTMANN, H. & KARLE, J. (1959). *Acta Cryst.* **12**, 846-850.
KUCAB, M. (1981). *Acta Cryst.* A**37**, 17-21.
LADD, M. F. C. & PALMER, R. A. (1980). Editors. *Theory and Practice of Direct Methods in Crystallography*, pp. 93-149. New York: Plenum Press.
ROLLEY-LE COZ, M., SENECHAL, M. & BILLETT, Y. (1983). *Acta Cryst.* A**39**, 74-76.
RUTHERFORD, J. S. (1992). *Acta Cryst.* Submitted.
RUTHERFORD, J. S., ROBERTSON, B. E., GUTTORMSON, R. J. & RUSSELL, D. B. (1988). *Can. J. Chem.* **66**, 655-661.

Acta Cryst. (1992). A**48**, 508-515

Analysis of Neutron Diffraction Data in the Case of High-Scattering Cells. II. Complex Cylindrical Cells

BY C. PETRILLO

Istituto di Struttura della Materia del Consiglio Nazionale delle Ricerche, Via E. Fermi 38, 00044 *Frascati, Italy*

AND F. SACCHETTI

Dipartimento di Fisica dell'Università di Perugia, Perugia, Italy

(*Received* 28 *May* 1991; *accepted* 17 *December* 1991)

Abstract

A new numerical program for the calculation of neutron scattering intensities in a complex cell made of n concentric cylinders has been developed with the purpose of analysing the diffraction data of fluid metals under high-temperature and high-pressure conditions. A simulation of the experiment on liquid Cs at $T = 1673$ K and $P = 86 \times 10^5$ Pa contained in such a cell has been performed in order to test the accuracy of standard data-analysis procedures employed to derive the static structure factor.

1. Introduction

In the last few years there has been a great deal of interest in the study of fluids at high pressures and/or elevated temperatures. Structural, thermodynamic and electronic properties of fluid metals up to their liquid-gas critical point have been investigated both experimentally (Hensel, Juengst, Noll & Winter, 1985; Freyland & Hensel, 1985) and theoretically (March, 1989, and references therein). Special experimental high-temperature high-pressure techniques have been developed in order to deal with the problem of containing highly corrosive metals in uncontaminated form in these extreme thermodynamic conditions. In particular, a quite complex cell has been designed for neutron diffraction studies in these systems (Freyland, Hensel & Glaser, 1979) and successfully employed for measurements of the static structure factor in liquid Cs ($T_c = 1924$ K, $P_c = 92.5 \times 10^5$ Pa) and Rb ($T_c = 2090$ K, $P_c = 140 \times 10^5$ Pa) (Franz, Freyland, Glaser, Hensel & Schneider, 1980; Freyland, Hensel & Glaser, 1984; Winter & Bodensteiner, 1988; Winter, Hensel, Bodensteiner & Glaser, 1987). The manufacture of such a cell opens the possibility of studying the microscopic properties of many fluids in critical conditions, even though the neutron scattering investigation turns out to be complex. As described in Freyland, Hensel & Glaser (1979), such a cell can be schematically depicted as a set of n concentric cylinders of different materials representing the sample container, the heater elements, the heat shields and the pressure vessel. High pressures at the sample can be established by using a relatively thin-walled sample container and, at the same time, compensating the internal sample pressure by surrounding the container with Ar gas under pressure (Freyland, Hensel & Glaser, 1979). Therefore, the compensating gas can be thought of as playing the role of an additional cylinder constituting the complex cell. The use of such a cell in a neutron diffraction measurement entails a high background contribution from the sample containment to the total scattered intensity. Therefore, accurate data treatment is necessary in order to derive the correct static structure factor $S(\mathbf{Q})$ from the measured intensities.

In a previous paper (Petrillo & Sacchetti, 1990), a data-reduction procedure applicable to neutron diffraction measurements in low-scattering-power fluids contained in high-scattering cells has been presented. The main purpose of that paper was to optimize the subtraction of contributions coming

0108-7673/92/040508-08$06.00

from the cell, accounting also for absorption and higher-order scattering processes involving the cell. The approach discussed in Petrillo & Sacchetti (1990) can be generalized to the case of n-cylinder geometry (Freyland, Hensel & Glaser, 1979) where the container subtraction appears to be a much more critical and complex point. A similar problem was discussed ten years ago by Soper & Egelstaff (1980). The present numerical approach, however, is completely different from that proposed by Soper & Egelstaff (1980) and the relative advantages will be discussed in the next section.

In the present paper we describe a new numerical program for the calculation of neutron scattering intensities and hence of the proper parameters occurring in the data-reduction procedure as applied to the general case of this cell geometry. Although the basic ideas of the previous numerical simulation remain the same, calculations are carried out using a rather different and optimized computational approach. In order to emphasize the importance of accounting for all the scattering processes from this system when analysing the diffraction data, a full simulation of a neutron diffraction experiment on liquid Cs at $T = 1673$ K and $P = 86 \times 10^5$ Pa (Winter & Bodensteiner, 1988) has been performed. By applying to the intensities simulated with the aid of the present program some standard data treatment based on Paalman & Pings (1962) and Blech & Averbach (1965) approaches, the effects introduced by an incorrect data analysis on the static structure factor are quantitatively discussed.

2. Data treatment and computational procedure

Typically, a neutron diffraction experiment to determine $S(\mathbf{Q})$ consists in performing five measurements: cell filled with the sample, empty cell, a full absorber, environment by removing sample and cell, and a vanadium standard. In this way, as discussed in Petrillo & Sacchetti (1990), it is possible to correct the data for the contributions from both the environment and the cell, for multiple scattering and for attenuation effects by making the maximum possible use of *measured* intensities and therefore reducing the effect of unavoidable inaccuracies due to sample and cell size and cross sections. A careful evaluation of the few unavoidable *calculated* parameters occurring in such a data treatment is however necessary. In the following, the basic equations of the data analysis developed by Petrillo & Sacchetti (1990) are briefly reported in a version generalized to treat the case of a sample contained in a high-pressure high-temperature cell like that schematically shown in Fig. 1 (Freyland, Hensel & Glaser, 1979). The notation employed throughout the present section is reported in Table 1. For the sake of simplicity, (1), (2) and (3) are developed to treat double-scattering processes even though higher-order terms can be calculated by the present version of the numerical program.

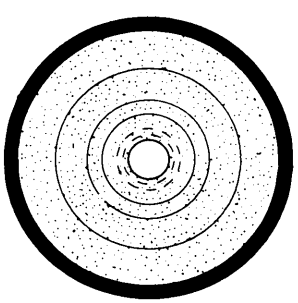

Fig. 1. Schematic transverse section of the high-temperature high-pressure cell described by Freyland, Hensel & Glaser (1979). Heavy full line: sample container (Mo, thickness = 0.3 mm); dashed lines: heaters (W, thickness = 0.05 mm); full lines: heat shields (Mo, thickness = 0.025 mm). The black area is the pressure vessel (aluminium alloy AlMgSi, thickness = 5 mm), the dotted areas are filled by Ar compensating gas.

Table 1. *Experimental and calculated neutron scattering intensities and calculated attenuation and transmission coefficients*

I_{s+c}^{exp}	experimental intensity from the sample inside the complex cell
I_c^{exp}	experimental intensity from the empty complex cell
I_{Cd}^{exp}	experimental intensity from a Cd bar inside the complex cell and having the same diameter as the sample container
I_a^{exp}	experimental intensity from the empty cell without the sample container
I_{s+c}^{B}	background intensity of the sample-plus-cell measurement
I_c^{B}	background intensity of the empty-cell measurement
I_s	single-scattering intensity from the sample
I_{ss}	double-scattering intensity from the sample
I_{ci}^{s}	single-scattering intensity from the ith cylinder constituting the cell filled with the sample
I_{ci}^{0}	single-scattering intensity from the ith cylinder constituting the cell without the sample
I_{cicj}^{s}	double-scattering intensity between the ith and the jth cylinders of the cell filled with the sample
I_{cicj}^{0}	double-scattering intensity between the ith and the jth cylinders of the cell without the sample
I_{sci}	double-scattering intensity between the sample and the ith cylinder of the cell
I_{cis}	double-scattering intensity between the ith cylinder of the cell and the sample
I_s^{corr}	single-scattering intensity from the sample corrected for the proper attenuation
T_s	sample attenuation coefficient accounting for the effects due to the sample and the whole cell

The measured total scattering intensities from the sample and from the empty container can be written as

$$I_{s+c}^{exp} = I_s + I_{ss} + \sum_i I_{ci}^{s} + \sum_{ij} I_{cicj}^{s} + \sum_i I_{sci} + \sum_i I_{cis} + I_{s+c}^{B}, \quad (1a)$$

$$I_c^{exp} = \sum_i I_{ci}^{0} + \sum_{ij} I_{cicj}^{0} + I_c^{B}. \quad (1b)$$

Such intensities contain the appropriate attenuation as suffered by neutrons in crossing both the sample and the n cylinders constituting the complex cell (see

Fig. 1). Empty cell and multiple-scattering contributions can be subtracted by defining respectively the calculated parameters γ and m, whose generalizations are

$$\gamma = \frac{\sum_i I^s_{ci} + \sum_{ij} I^s_{cicj}}{\sum_i I^0_{ci} + \sum_{ij} I^0_{cicj}} \qquad (2a)$$

$$m = \left[\left(I_{ss} + \sum_i I_{sci} + \sum_i I_{cis}\right) \Big/ \lim_{Q\to\infty} I_s\right]. \qquad (2b)$$

The single-scattering intensity from the sample, corrected for all the attenuation effects, is given by

$$\begin{aligned} I_s^{\rm corr} &= I_s / T_s \\ &= \{I^{\rm exp}_{s+c} - I^B_{s+c} - \gamma(I^{\rm exp}_c - I^B_c) - m/(m+1) \\ &\quad \times [I^{\rm exp}_{s+c} - I^B_{s+c} - \gamma(I^{\rm exp}_c - I^B_c)]_{Q\to\infty}\}/T_s. \end{aligned} \qquad (3)$$

In (2b) and (3) the notation $Q\to\infty$ means that multiple-scattering subtraction, as well as normalization to the standard, should be performed in that high-Q region where the trend of I_s can be reasonably modelled including the Q dependence due to inelasticity effects (for example, the sample cross section is smooth enough and no structural information is present).

Some observations deserve the definitions of background transmissions, entering the background intensities I^B_{s+c} and I^B_c, and of sample attenuation T_s. With an optical arrangement in which only some of the cylinders are 'seen' by the neutron detector, the background transmission is given by

$$T^B = \int_{-R_{\rm max}}^{R_{\rm max}} {\rm d}y \exp[-X(y)] D(y), \qquad (4a)$$

where $X(y)$ is the path integral of the total linear attenuation coefficient along a straight line parallel to the incoming neutron-beam direction, y is a coordinate along a direction perpendicular to that of the beam, $R_{\rm max}$ is the radius of the outermost cylinder (*i.e.* the pressure vessel) and $D(y)$ is a function normalized to unity accounting for the detector optics. For example, with a rectangular shape assumed for $D(y)$, *i.e.* $D(y) = 1/2R_i$ if $y < R_i$, $D(y) = 0$ if $y > R_i$, only the background neutrons crossing the cylindrical volumes with radii smaller than R_i will be collected by the detector. Therefore, the integration in (4a) is performed over an appropriate cylinder diameter accounting for the optics of the detector, while the path integral $X(y)$ is performed over the outermost cylinder diameter since all the cylinders contribute anyway to attenuate the background neutrons collected by the detector.

The attenuation suffered by the neutron beam during single-scattering processes at different scattering angles is still defined by equation (11) of Petrillo & Sacchetti (1990) when the system is fully bathed by the beam. When such a condition is not verified, the effect of the finite size of the incoming beam has to be taken into account and the attenuation is modified as

$$T = \int {\rm d}\mathbf{r}\, J_0(\mathbf{r}) \exp[-(X_I + X_F)] \Big/ \int {\rm d}\mathbf{r}\, J_0(\mathbf{r}) \qquad (4b)$$

where X_I and X_F are the path integrals of the total linear attenuation coefficient along the path lengths of the incoming and scattered neutron beams and $J_0(\mathbf{r})$ is a function describing the transverse shape of the incoming neutron beam.

The effect of a finite beam size has to be taken into account also when defining the intensities associated with single- (I^1) and multiple- (I^n, $n>1$) scattering processes entering the calculation of the parameters γ and m [(2a) and (2b)]. In particular, one has

$$I^1_\alpha = N_\alpha ({\rm d}\sigma/{\rm d}\Omega)_\alpha \int_{V_\alpha} {\rm d}\mathbf{r}\, J_0(\mathbf{r}) \times \exp[-(X_I + X_F)] \Big/ \int_{V_\alpha} {\rm d}\mathbf{r}\, J_0(\mathbf{r}), \qquad (5a)$$

$$\begin{aligned} I^n_{\alpha 1\ldots\alpha_n} &= \int_{V_{\alpha 1}} {\rm d}\mathbf{r}_1\, J_0(\mathbf{r}_1) N_{\alpha 1} ({\rm d}\sigma/{\rm d}\Omega)_{\alpha 1} \Big/ \int_{V_{\alpha 1}} {\rm d}\mathbf{r}\, J_0(\mathbf{r}) \\ &\quad \times \prod_{i=2}^{n} \left[N_{\alpha i} ({\rm d}\sigma/{\rm d}\Omega)_{\alpha i} \right. \\ &\quad \left. \times \int_{V_{\alpha i}} {\rm d}\mathbf{r}_i \exp\left(-X_I - X_F - \sum_{k=1}^{n-1} X_k\right) \Big/ \prod_{j=1}^{n-1} L_j^2 \right] \end{aligned} \qquad (5b)$$

where the index α refers to the sample or the general cylinder and V_α is the corresponding volume, N_α is the number density and $({\rm d}\sigma/{\rm d}\Omega)_\alpha$ the differential cross section. X_k is the integral along the path I_k between kth and $(k+1)$th scattering events. Finally, we note that the detector optics, described by the function $D(y)$, can be easily inserted into (4b), (5a) and (5b).

The application of the present data treatment (1a)–(4b) to the neutron scattering intensities collected using such a high-pressure high-temperature cell needs however some additional comments. A first question regards the 'full-absorber' measurement which is required in order to evaluate the background intensities I^B_{s+c} and I^B_c (Petrillo & Sacchetti, 1990). In principle, such a measurement is intended to account for all the scattering processes originating from the environment when the neutron paths do not cross the volume otherwise occupied by the system sample plus cell. Therefore the dimensions of the absorber are dictated by height and external diameter of the cell. Adopting this prescription in the case of the cell shown in Fig. 1 would require a measurement on an absorber bar having the same diameter as the outer pressure vessel. In this condition, the formulas defining I^B_{s+c} and I^B_c developed by Petrillo & Sacchetti

(1990) remain valid. In contrast, deviations from this 'dimension prescription' for the full absorber would imply some obvious modifications of the basic equations.

A second problem is related to the 'empty-cell' measurement. As already discussed, the Ar gas necessary to compensate the high pressure at the sample has to be considered as an additional cylindrical volume constituting the complex cell. Indeed, when measuring the sample, the contributions to the intensity coming from the compensating gas could be not negligible and in principle should be subtracted as part of the 'empty-cell' contribution. Of course, removing the sample entails removing the Ar gas unless substituting the sample with a virtually zero-scattering gas having the only function of keeping the whole system under Ar pressure during the 'empty-cell' measurement.

3. Computational procedure

The calculation of the scattering intensities defined by the integrals (5*a*) and (5*b*) has been carried out using the same approach as described by Petrillo & Sacchetti (1990), namely a Monte Carlo (MC) integration procedure in which a random sampling of the integration volume is performed. Given a couple of scattering points randomly sampled inside the total volume, one must univocally associate a value of the total linear attenuation coefficient with each point and then calculate the path lengths associated with both single- and multiple-scattering processes involving the given couple of points. Path lengths are evaluated using a subroutine which makes the search for the interception points between the straight lines of the neutron path and all the relevant cylindrical surfaces. The geometrical problem of finding the interception points is simplified by using a parametrized form for the straight line, *i.e.*

$$\begin{aligned} x &= x_1 + t(x_2 - x_1) \\ y &= y_1 + t(y_2 - y_1) \quad \text{with } 0 \le t \le 1. \\ z &= z_1 + t(z_2 - z_1) \end{aligned}$$

The condition $0 \le t \le 1$ automatically guarantees that the interception points are contained inside the total volume. The subroutine thus yields the values of the parameters t, ordered from the lowest to the highest value, for every couple of points (x_1, y_1, z_1) and (x_2, y_2, z_2). With known paths and related total linear attenuation coefficients, as well as the appropriate cross section of the material depending on the scattering angle, the integrals (5*a*) and (5*b*) are easily evaluated.

A detailed discussion about the errors on γ and m introduced by inaccuracies of the MC integration procedure has been presented by Petrillo & Sacchetti (1990) for the two-cylinder geometry. The generalization to n cylinders does not alter substantially this discussion. The only difference in the present case is that, as the number of sampling points inside each cylinder is proportional to its volume, an adequate sampling in each volume generally requires the use of a high total number of random points. Of course, the choice of such a number depends on the number of cylinders constituting the cell and on the values of their volumes. As an example, we report in Table 2 the values of the parameters γ [(2*a*)], m [(2*b*)] and T_s [(4*c*)] calculated in the case of a hypothetical four-cylinder geometry as a function of both the total number of sampling points and the cylinder volumes. In order to study the statistical stability of γ and m values *versus* the number of sampling points as related to the cylinder volumes, the calculations have been performed at a fixed scattering angle and assuming a homogeneous incoming beam bathing the whole system.

Table 2. *Calculated γ, m and T_s parameters as a function of the number of iterations in a hypothetical four-cylinder system with a varying volume*

R: radius of the cylinder; μ^{tot}: total linear attenuation coefficient. Calculations have been performed at fixed scattering angle $2\theta = 50°$ and for a homogeneous incoming beam bathing the whole system. No 'small-path' correction has been applied in the calculation (see text).

			Number of iterations		
R (cm)	μ^{tot} (cm^{-1})		3×10^5	6×10^5	9×10^5
0.50	0.5				
0.55	0.3	γ	0.932	0.931	0.931
2.50	0.005	m	0.308	0.329	0.316
2.55	0.4	T_s	0.598	0.600	0.600
0.50	0.5				
0.65	0.3	γ	0.946	0.944	0.945
2.50	0.005	m	0.479	0.498	0.485
2.55	0.4	T_s	0.457	0.459	0.459

Finally, we note that possible inaccuracies in the calculation of multiple-scattering intensities [(5*b*)] can originate from small paths I_k between kth and $(k+1)$th scattering points randomly generated. The diverging behaviour of the integrand function in (5*b*) can introduce a numerical instability (of the order of 0.01 or less) in the calculated value of the parameter m as a function of the number of sampling points. On the contrary, this problem is completely overwhelmed in the case of the γ parameter which is calculated as a ratio of homogeneous quantities, that is the effect of 'small paths' is equally contributing to both the numerator and the denominator and therefore largely cancels. In order to reduce this numerical effect, we introduced a correction described in the Appendix. A check of the goodness of such a correction has been done by running the program, modified to account for this effect, in the case of the two hypothetical systems of Table 2. Quite satisfactory results for m are found; in particular, when the number of sampling points is increased from 3×10^5 to

6×10^5 and to 9×10^5, the value of m changes from 0.312 to 0.319 and to 0.317 for the first system and from 0.489 to 0.487 and to 0.487 for the second system. The use of this 'small-paths' corrective function is, however, not recommended in the case of extremely reduced thicknesses of both sample and containers, where this concept is no longer meaningful.

Finally, we mention the advantages that the present computational method has over the more conventional one used by Soper & Egelstaff (1980). Firstly, in the present approach the computing effort is proportional to the scattering order while in the conventional procedure it follows a power law. Moreover, the present approach allows for the use of a rather large number of sampling points within the integration volume so that good accuracy can be obtained in the correction of the diverging behaviour of the integrand in (5*b*). The advantage of having a large number of sampling points is very well exploited in the case of complex cells when rather thin metallic cylinders giving a non-negligible contribution are present.

4. Results and discussion

The present program, whose principal application is the calculation of parameters γ, m and T_s when analysing the experimental data, has been used to simulate a neutron scattering experiment on a hard-sphere liquid contained in the complex cell shown in Fig. 1. In particular, the simulation has been performed with reference to liquid Cs at $T=1673$ K and $P=86\times10^5$ Pa whose experimental data are reported by Winter & Bodensteiner (1988). In order to simulate the experimental intensities $I_{s+c}^{\exp}$, $I_c^{\exp}$, I_{s+c}^{B} and I_c^{B} [(1*a*) and (1*b*)], the intensities of single- [(5*a*)] and double- [(5*b*)] scattering processes taking place within the whole system of sample plus complex cell were calculated using the values of linear attenuation coefficients reported in Table 3. All the components of the cell apart from the sample were treated as isotropic scatterers. The differential cross section of liquid Cs appearing in (5*a*) and (5*b*) was obtained, neglecting the incoherent scattering, by $d\sigma/d\Omega = Nb^2S(Q)$ where $N=0.0044$ atoms Å^{-3} is the number density at $T=1673$ K and $P=86\times10^5$ Pa (Winter & Bodensteiner, 1988) and $b=5.42$ fm is the coherent scattering length. The static structure factor $S(\mathbf{Q})$ was calculated using the Percus–Yievick approximation (Ziman, 1982) assuming a hard-sphere radius of 4.8 Å and no inelasticity effect was taken into account. The values of the cross sections employed in the calculation of the linear attenuation coefficients were taken from McLane, Dunford & Rose (1988). The density of the Ar compensating gas was calculated according to the perfect-gas law using a value of pressure equal to 86×10^5 Pa and temperature values changing from 1673 K at the centre of the cell down to room temperature at the pressure vessel. Quite reasonably, it can be assumed that the temperature remains almost constant over the distance from the centre of the cell to the first heat shield, reduces by about a factor of two in passing from the first to the second heat shield and decreases smoothly to room temperature at the pressure-vessel radius. All the calculations were performed at an incoming neutron wavelength of 0.7 Å and an incident-beam height of 5 cm. The incoming beam profile was simulated by a Gaussian beam shape having a full width at half-maximum (FWHM) of 1 cm. Some information about the contributions to the scattered intensity coming from the different components of the cell can be inferred by the data reported in Table 4 where the ratio of single scattering from sample container, heaters, heat shields, compensating gas and pressure vessel to single scattering from the sample are reported as a function of the scattering angle.

Table 3. *Radii and linear attenuation coefficients related to scattering (μ^{scat}) and absorption (μ^{abs}) cross sections for the different components of the cell shown in Fig. 1*

Absorption cross sections refer to an incoming neutron wavelength $\lambda=0.7$ Å.

	R (cm)	μ^{scat} (cm^{-1})	μ^{abs} (cm^{-1})
Cs	0.750	0.0172	0.0492
Mo	0.780	0.39	0.033
Ar	0.950	0.0003	0.0001
W	0.955	0.358	0.45
Ar	1.170	0.0003	0.0001
W	1.175	0.358	0.45
Ar	1.720	0.0005	0.0002
Mo	1.723	0.39	0.033
Ar	2.265	0.0011	0.0004
Mo	2.268	0.39	0.033
Ar	3.438	0.012	0.0005
Mo	3.440	0.39	0.033
Ar	4.350	0.0146	0.0006
AlMgSi	4.85	0.091	0.0054

In Fig. 2 the simulated 'experimental' intensities from the sample contained in the complex cell ($I_{s+c}^{\exp}$), from the empty cell ($I_c^{\exp}$), from the cell after removing sample and sample container ($I_a^{\exp}$) and from a cadmium bar having the same diameter as the sample container ($I_{Cd}^{\exp}$) are shown as functions of the scattering angle. The choice of simulating such intensities, and not for example that of a cadmium bar with the same diameter as the outer one of the pressure vessel, was dictated by the attempt to reproduce as closely as possible the experiment presented by Winter & Bodensteiner (1988). Following this paper, we define the background intensities I_{s+c}^{B} and I_c^{B} as

$$I_{s+c}^{B}=I_{Cd}^{\exp}+A_{s,sc}(I_a^{\exp}-I_{Cd}^{\exp}),$$

$$I_c^{B}=I_{Cd}^{\exp}+A_{c,c}(I_a^{\exp}-I_{Cd}^{\exp}),$$

where the terms A_{ij} are the cylindrical absorption factors described in Paalman & Pings (1962). The corrected single-scattering intensity from the sample,

Table 4. *Ratios of single-scattering intensities from the sample container (I_2), the two heaters (I_3), the three heat shields (I_4), all the* Ar *compensating gas (I_5), the pressure vessel (I_6) and the single-scattering intensity from the sample (I_1) at three values of the scattering angle 2θ*

2θ (°)	I_2/I_1	I_3/I_1	I_4/I_1	I_5/I_1	I_6/I_1
0	1.3	0.39	0.30	0.37	4.4
50	1.3	0.39	0.31	0.39	4.6
100	1.3	0.40	0.31	0.39	4.3

I_s^{corr}, was then obtained by applying to the simulated intensities the Paalman & Pings (1962) and Blech & Averbach (1965) corrections. One has

$$I_s^{corr} = [I_{s+c}^{exp} - I_c^{exp} A_{c,sc}/A_{c,c}]/A_{s,sc} - \Delta/(\Delta+1)[I_{s+c}^{exp} - I_c^{exp} A_{c,sc}/A_{c,c}]/A_{s,sc}, \quad (6)$$

where $\Delta = \delta(\sigma^{scat}/\sigma^{tot})$, δ defined in Blech & Averbach (1965), $\sigma^{scat} = 3.95\times10^{-28}$ m^2 and $\sigma^{tot} = 15.26\times10^{-28}$ m^2 being the scattering and total (scattering plus absorption) cross sections. The absorption factors A_{ij} are calculated only on sample and sample-container volumes, that is ignoring the attenuation effects due to heaters, heat shields, Ar gas and pressure vessel. Moreover, the multiple scattering is assumed to take place only within the sample, that is neglecting all the multiple processes taking place among the sample and the n cylinders constituting the cell. In Table 5 the A_{ij} factors and the δ parameter employed in the calculation are reported. As discussed by Petrillo & Sacchetti (1990), for a two-cylinder geometry, the $A_{s,sc}$ and the $A_{c,sc}$ parameters are respectively equal to the sample and the cell attenuation factors calculated by (4*b*). The $A_{c,c}$ parameter is, on the other hand, obtained from (4*b*) evaluated for the specific case of the empty cell.

Table 5. *Paalman & Pings* (1962) *coefficients A_{ij} as a function of the scattering angle 2θ calculated for liquid* Cs *at $T = 1673$ K and $P = 86\times10^5$ Pa contained in the* Mo *sample container*

δ is the double-scattering parameter defined by Blech & Averbach (1965).

2θ (°)	$A_{s,sc}$	$A_{c,c}$	$A_{c,sc}$	$A_{c,sc}/A_{c,c}$	δ
0	0.891	0.947	0.891	0.941	0.053
20	0.891	0.947	0.891	0.941	
40	0.891	0.947	0.892	0.942	
60	0.891	0.947	0.892	0.942	
80	0.891	0.947	0.893	0.943	
100	0.891	0.947	0.893	0.943	
120	0.891	0.947	0.894	0.944	
140	0.892	0.947	0.894	0.944	

The corrected single-scattering intensity obtained from (6) is shown in Fig. 3 in comparison with the ideal single-scattering intensity for liquid Cs. As we see, an average difference of about 15% is found between the two corrected intensities which has to be attributed to the data-reduction procedure. On the other hand, a more realistic estimation of the multiple scattering accounting for processes also involving the cell would increase such a contribution with the consequence of further lowering the reconstructed intensity. The observed difference is due to both an incorrect cell subtraction and sample attenuation correction as obtained by applying the Paalman & Pings (1962) method. In particular, the difference between

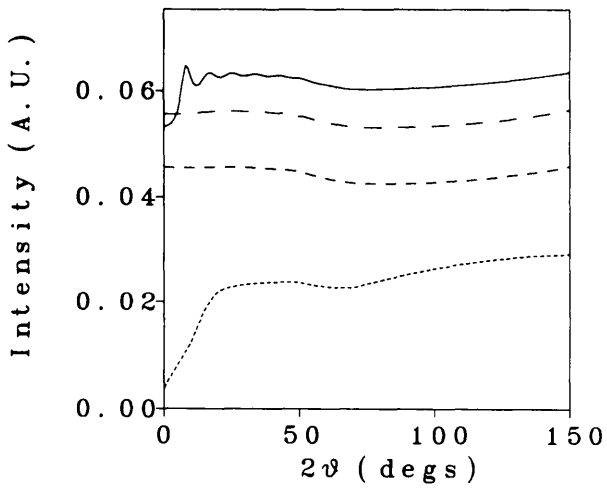

Fig. 2. Simulated 'experimental' intensities (arbitrary units) *versus* scattering angle 2θ. Full line: sample inside the complex cell (I_{s+c}^{exp}); dashed line: empty cell (I_c^{exp}); short-dashed line: empty cell after removing sample and sample container (I_a^{exp}); dotted line: cadmium bar having the same diameter as the sample container put inside the cell (I_{Cd}^{exp}).

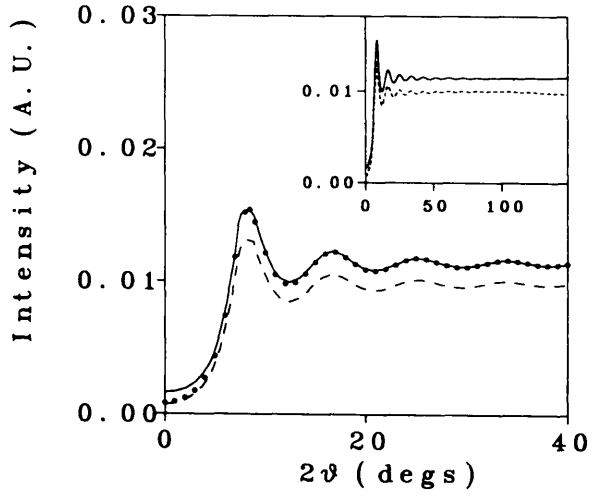

Fig. 3. Single-scattering intensities from liquid Cs at $T = 1673$ K and $P = 86\times10^5$ Pa (arbitrary units) *versus* scattering angle 2θ. Full line: ideal intensity; dashed line: reconstructed intensity after Paalman & Pings (1962) and Blech & Averbach (1965) corrections to the simulated 'experimental' intensities; dots: reconstructed intensity normalized to the ideal one. The insert shows the same functions over a wider scattering-angle range.

Table 6. γ, m and T_s parameters calculated for the present simulated 'experiment' as a function of the scattering angle

2θ (°)	γ	m	T_s
0	0.925	0.069	0.780
10	0.941	0.069	0.780
20	0.953	0.069	0.780
40	0.955	0.069	0.780
60	0.956	0.069	0.780
80	0.958	0.069	0.781
100	0.961	0.069	0.781
150	0.958	0.069	0.781

the Paalman & Pings (1962) coefficient $A_{s,sc}$, which neglects the attenuation effects due to the outer cylinders, and the present sample attenuation T_s is almost totally responsible for the observed discrepancy. For the sake of comparison, we report in Table 6 the values of γ, m and T_s calculated for the present 'experiment' as a function of the scattering angle. The difference between these values and the Paalman & Pings (1962) calculation gives a quantitative indication of the attenuation effect introduced by all the other cylinders, that is heaters, heat shields, compensating gas and pressure vessel.

Finally, in Fig. 3, the reconstructed intensity normalized by the ideal intensity at high angles (130–150°), where no structure is visible (see the insert of Fig. 3), is also shown. Even though such a normalization removes the 15% discrepancy, residual differences in the region before the first peak and around the first minimum are still present. In particular, the discrepancy at low angles ($2\theta \leq 10°$) has to be related to the cell subtraction which in the Paalman & Pings (1962) approach is done by multiplying the cell contribution by the ratio $A_{c,sc}/A_{c,c}$. Such a ratio plays the role of the γ parameter [see (3)]. At low angles the sample obscures those scattering contributions coming from the outer cylinders much more than at higher angles. This effect is accounted for by the angular dependence of the γ parameter (see Table 6) whereas the ratio $A_{c,sc}/A_{c,c}$ is constant at low angles. Therefore, the cell subtraction is overestimated by the Paalman & Pings (1962) approach exactly in the low-angle region which is of importance when studying the structure of the fluid under high pressure (Winter & Bodensteiner, 1988).

The data reduction and the numerical procedure described here have already been applied to the analysis of neutron diffraction data from liquid Cl_2 at 412 K where a quartz sample container enclosed in a vanadium pressure vessel with ^{4}He compensating gas was employed (Bellissent-Funel, Buontempo, Petrillo & Ricci, 1991).

We thank one of the referees for his very accurate reading of the paper and for his helpful comments and suggestions.

APPENDIX

In order to cope with the problem of the divergences in the integrand of (5*b*), one can observe that the typical integral which has to be performed can be written as

$$I = \int_V \mathbf{dr} \int_V \mathbf{dr}' \exp[-F(\mathbf{r}, \mathbf{r}')]/|\mathbf{r}-\mathbf{r}'|^2. \quad (A1)$$

With the introduction of the variable $\mathbf{x} = \mathbf{r} - \mathbf{r}'$, (*A*1) becomes

$$I = \int_V \mathbf{dr} \int_{V_{x(\mathbf{r})}} \mathbf{dx} \exp[-F(\mathbf{r}, \mathbf{r}-\mathbf{x})]/x^2, \quad (A2)$$

where $V_{x(\mathbf{r})}$ is the transformed volume for the $\mathbf{x}$ variable. The integral on $V_{x(\mathbf{r})}$ can be split according to

$$V_{x(\mathbf{r})} = V_1 + V_2 \quad (A3)$$

with

V_1: volume such that $x \geq x_0$,

V_2: volume such that $x \leq x_0$,

and x_0 is small enough to guarantee with an appropriate accuracy:

$$\exp[-F(\mathbf{r}, \mathbf{r}-\mathbf{x})] = \exp[-F(\mathbf{r}, \mathbf{r})]$$

when $\mathbf{x}$ is contained in V_2. Therefore, one gets

$$I = \int_V \mathbf{dr} \int_{V_1} \mathbf{dx} \exp[-F(\mathbf{r}, \mathbf{r}-\mathbf{x})]/x^2 + \int_V \mathbf{dr} \exp[-F(\mathbf{r}, \mathbf{r})] \int_{V_2} \mathbf{dx}\, 1/x^2. \quad (A4)$$

The volume V_2 can be small enough to be approximated by a sphere of radius $R_0 = [3V_2/(4\pi)]^{1/3}$, so that one gets

$$I = \int_V \mathbf{dr} \int_{V_1} \mathbf{dx} \exp[-F(\mathbf{r}, \mathbf{r}-\mathbf{x})]/x^2 + 4\pi R_0 I_1, \quad (A5)$$

where I_1 is an integral which must be performed in order to calculate the single-scattering contribution, so that no further computing time is required to evaluate (*A*5). On the other hand, no diverging behaviour is present in the first term of (*A*5).

References

BELLISSENT-FUNEL, M. C., BUONTEMPO, U., PETRILLO, C. & RICCI, F. P. (1991). *Mol. Phys.* **74**, 1209–1220.

BLECH, I. A. & AVERBACH, B. L. (1965). *Phys. Rev. A*, **137**, 1113–1116.

FRANZ, G., FREYLAND, W., GLASER, W., HENSEL, F. & SCHNEIDER, E. (1980). *J. Phys. Colloq.* C8, **41**, 194–198.

FREYLAND, W. & HENSEL, F. (1985). In *The Metallic and Non-metallic States of Matter. An Important Facet of Chemistry and Physics of Condensed Matter*, edited by P. P. EDWARDS & C. N. R. RAO. London: Taylor and Francis.

FREYLAND, W., HENSEL, F. & GLASER, W. (1979). *Ber Bunsenges. Phys. Chem.* **83**, 884–889.

FREYLAND, W., HENSEL, F. & GLASER, W. (1984). *Rev. Phys. Appl.* **19**, 747–749.

HENSEL, F., JUENGST, S., NOLL, F. & WINTER, R. (1985). In *Localization and Metal-Insulator Transitions*, edited by D. ADLER & H. FRITZSCHE. New York: Plenum.
MCLANE, V., DUNFORD, C. L. & ROSE, P. F. (1988). *Neutron Cross Sections*, Vol. 2. London: Academic Press.
MARCH, N. H. (1989). *Phys. Chem. Liq.* **20**, 241-245.
PAALMAN, H. H. & PINGS, C. J. (1962). *J. Appl. Phys.* **33**, 2635-2639.
PETRILLO, C. & SACCHETTI, F. (1990). *Acta Cryst.* A**46**, 440-449.
SOPER, A. K. & EGELSTAFF, P. A. (1980). *Nucl. Instrum. Methods*, **178**, 415-425.
WINTER, R. & BODENSTEINER, T. (1988). *High Press. Res.* **1**, 23-37.
WINTER, R., HENSEL, F., BODENSTEINER, T. & GLASER, W. (1987). *Ber. Bunsenges. Phys. Chem.* **91**, 1327-1330.
ZIMAN, J. M. (1982). *Models of Disorder*. Cambridge Univ. Press.

Acta Cryst. (1992). A**48**, 515-532

Bravais Classes for the Simplest Incommensurate Crystal Phases

BY N. DAVID MERMIN AND RON LIFSHITZ

Laboratory of Atomic and Solid State Physics, Cornell University, Ithaca, NY 14853-2501, *USA*

(*Received* 19 *September* 1991; *accepted* 10 *January* 1992)

Abstract

Through the reformulation of crystallography that treats periodic and quasiperiodic structures on an equal footing in three-dimensional Fourier space, a novel computation is given of the Bravais classes for the simplest kinds of incommensurately modulated crystals: (3+3) Bravais classes in the cubic system and (3+1) Bravais classes in any of the other six crystal systems. The contents of a Bravais class are taken to be sets of ordinary three-dimensional wave vectors inferred from a diffraction pattern. Because no finer distinctions are made based on the intensities of the associated Bragg peaks, a significantly simpler set of Bravais classes is found than Janner, Janssen & de Wolff [*Acta Cryst.* (1983). A**39**, 658-666] find by defining their Bravais classes in higher-dimensional superspace. In our scheme, the Janner, Janssen & de Wolff categories appear as different ways to describe identical sets of three-dimensional wave vectors when those sets contain crystallographic (3+0) sublattices belonging to more than a single crystallographic Bravais class. While such further discriminations are important to make when the diffraction pattern is well described by a strong lattice of main reflections and weaker satellite peaks, by not making them at the fundamental level of the Bravais class, the crystallographic description of all quasiperiodic materials is placed on a single unified foundation.

I. Introduction

Two approaches have been proposed for extending to quasiperiodic structures the conventional crystallographic description of periodic materials. The older superspace approach* retains the fundamental role of periodicity. By regarding quasiperiodic structures as three-dimensional sections of structures periodic in a higher $(3+d)$-dimensional space, it extracts their classification scheme by examining the ordinary crystallographic categories of periodic structures in $(3+d)$ dimensions. The second approach,† developed more recently in response to the discovery of icosahedral and decagonal quasicrystals, abandons the traditional reliance on periodicity and reformulates ordinary crystallography in three dimensions in a way that embraces quasiperiodic materials from the start.

In the three-dimensional approach which dethrones periodicity, a unified crystallography of periodic and quasiperiodic materials emerges as a symmetry-based classification scheme for diffraction patterns consisting of sharp Bragg peaks.‡ When those diffraction patterns can be indexed by three integers, the general scheme reduces to the ordinary crystallographic space-group classification of periodic structures; but the same three-dimensional scheme works just as well for the diffraction patterns

* Our results here bear most directly on the formulations given in de Wolff, Janssen & Janner (1981) and Janner, Janssen & de Wolff (1983). For a recent review see Janner (1991).

† For recent reviews see Rabson, Mermin, Rokhsar & Wright (1991) and Mermin (1992).

‡ The advantages of working in Fourier space even in the periodic case were first emphasized by Bienenstock & Ewald (1962), but it is only in the last dozen years, with the great interest in incommensurately modulated crystals and quasicrystals, that the need has become acute for such a radical reformulation of the foundations of crystallography.

0108-7673/92/040515-18$06.00